

The glass transition and the non-Arrhenian viscosity of carbonate melts

DONALD B. DINGWELL¹, KAI-UWE HESS^{1,*}, MARTIN C. WILDING^{2,5}, RICHARD A. BROOKER³,
DANILO DI GENOVA³, JAMES W.E. DREWITT³, MARK WILSON⁴, AND DANIEL WEIDENDORFER¹

¹Earth and Environmental Sciences, Ludwig-Maximilians-Universität München, Theresienstraße 41/III, 80333 München, Germany

²Materials and Engineering Research Institute, Sheffield Hallam University, Howard Street, Sheffield, S1 1WB, U.K.

³School of Earth Sciences, Wills Memorial Building, Queens Road, Bristol, BS8 1RJ, U.K.

⁴Department of Theoretical Chemistry, University of Oxford, South Parks Road, Oxford, OX1 1U.K.

⁵U.K. Catalysis Hub, Research Complex at Harwell, Rutherford Appleton Laboratory, Harwell, OX11 0DE, U.K.

ABSTRACT

We report the first calorimetric observation of the glass transition for a carbonate melt. A carbonate glass [55K₂CO₃–45MgCO₃ (molar)] was quenched from 780 °C at 0.1 GPa. The activation energy of structural relaxation close to the glass transition was derived through a series of thermal treatments comprising excursions across the glass transition at different heating rates. Viscosities just above the glass transition temperature were obtained by applying a shift factor to the calorimetric results. These viscosity measurements (in the range of 10⁹ Pa·s) at supercooled temperatures (ca. 230 °C) dramatically extend the temperature range of data for carbonates, which were previously restricted to superliquidus viscosities well below 1 Pa·s. Combining our calorimetrically derived results with published alkaline-earth carbonate melt viscosities at high temperatures yields a highly non-Arrhenian viscosity-temperature relationship and confirms that carbonate liquids are “fragile.” Based on simulations, fragile behavior is also exhibited by Na₂CO₃ melt. In both cases, the fragility presumably relates to the formation of temperature-dependent low-dimensional structures and Vogel-Fulcher-Tammann (VFT) curves adequately describe the viscosity-temperature relationships of carbonate melts below 1000 °C.

Keywords: Viscosity, glass transition, fragility, carbonate melt, carbonatite, shift factor

INTRODUCTION

Melt viscosity has a fundamental control on many Earth processes, from how melts are transported through the deep mantle and crust, to its influence on effusive or explosive eruption styles at the Earth surface (McKenzie 1985; Dingwell 1996). Although physical properties (e.g., viscosity, density, surface tension) are becoming well-established for multicomponent silicate systems of importance in earth sciences (Lange and Carmichael 1987; Knoche et al. 1995; Bagdassarov et al. 2000; Giordano et al. 2008), carbonate melts are less well-studied in the geosciences, due to relatively rare volcanic expression at the Earth’s surface (Keller 1989; Dawson 1966). Carbonate volcanism is nevertheless a part of the Earth system and may be more common on other planets. Carbonatite volcanism has been invoked for so-called “canali”—channels on Venus, which reach up to 6800 km in length, implying a very low-viscosity flow (Kargel et al. 1994). Highly mobile carbonatite melts migrating within the Earth likely play a major role as metasomatizing agents (Blundy and Dalton 2000; Hammouda and Laporte 2000) and in the subduction-related recycling of carbon back to Earth’s surface as part of the global carbon cycle (Dasgupta and Hirschmann 2010; Thomson et al. 2016). Their ability to scavenge high concentrations of REE and rare metals make them increasingly important as multi-commodity exploration targets for the green energy

revolution (Simandl and Paradis 2018). The extreme physical and chemical properties (e.g., density, viscosity, conductivity, reactivity), which set carbonatites apart from most silicate melts, must have a strong influence on the interaction and migration dynamics of buoyant carbonatite melts throughout the lithosphere after separating from their source region (Hunter and McKenzie 1989; Minarik and Watson 1995; Brooker 1998; Hammouda and Laporte 2000; O’Leary et al. 2015). The relationship between low viscosity and electrical properties of carbonate-rich melts has also been linked to regions of high conductivity in the upper and lower mantle (Sifré et al. 2014; Gaillard et al. 2008).

These physical properties also have commercial applications, particularly in the design of molten carbonate fuel cells, which generally offer a prospect of greener electricity but may now also be designed with a capacity to efficiently capture CO₂ derived from the liquid, gaseous, or solid hydrocarbon (i.e., coal) fuel used for generating electricity (Cassir et al. 2012). Such molten carbonates generally provide excellent performance at low cost in thermal energy storage or heat transfer fluid systems (Wu et al. 2011).

Recent investigations of carbonate melt at the molecular scale have revealed a temperature- and pressure-dependence of structure that likely affects physical properties (Wilding et al. 2016, 2019a, 2019b; Wilson et al. 2018). Thus, a more complete understanding of the relationship between carbonate melt structure and physical properties is required. Here, we provide the first ever calorimetric determination of the glass

* E-mail: hess@lmu.de. Orcid 0000-0003-1860-8543

 Open access: Article available to all readers online.

transition of a carbonate glass and generate a direct measurement of the viscosity of a carbonate liquid just above the glass transition interval. In this manner we are able to constrain the non-Arrhenian temperature-dependence and thereby the fragility of molten carbonates, providing a parameterization valuable for the extrapolation and interpolation in temperature of the transport properties of carbonates.

Viscosity data: The carbonate challenge

Natural carbonatites are mainly composed of alkaline-earth (Ca, Mg, and Fe) alkali (Na and K) carbonates. Rheological measurements on the most geologically relevant end-member carbonates have proven difficult. This is especially true for alkaline earth carbonates as they do not melt congruently at atmospheric pressure (1 atm). For example, CaCO_3 decarbonates to $\text{CaO}+\text{CO}_2$ below 0.004 GPa and 1240 °C and then melts incongruently (to CaCO_3+CaO - or $\text{CaCO}_3+\text{CO}_2$ -rich melts) up to 0.3 GPa and 1375 °C. Only above this pressure and temperature is congruent melting observed (Smyth and Adams 1923; Wyllie and Huang 1976). For MgCO_3 and FeCO_3 the conditions are even more extreme (see Wyllie and Huang 1976; Weidner 1972). Viscosity measurements are less complicated for the alkali carbonates, as they melt congruently at atmospheric pressure, although they can be subject to dissociative CO_2 loss whose intensity decreases in the order $\text{Li} \gg \text{Na} > \text{K}$ (Janz and Lorenz 1961).

In Figure 1a, the ambient pressure, single alkali carbonate measurements imply a clear compositional effect of the different alkali cations, but large scatter also exists even within a single study. As is typically observed for very restricted ranges

of temperature and viscosity, all data [except (L,N,K)C] can be described within error by an Arrhenian temperature dependence (a linear fit on a $\log_{10} \eta$ vs. $1/T$ plot). As later noted by Janz et al. (1989), their initial “NIST standard” viscosity data were incorrect (and therefore are not included in Fig. 1a). For Na_2CO_3 they defer to the data of Ejima et al. (1984), which has a less steep slope, almost identical to the Sato et al. (1999) data in Figure 1a. Janz et al. (1989) suggest that the error and differences in general arise from comparisons of various measurement methods, experimental assemblies, and working equations, as well as matters of sample pre-treatments and impurities. Also included in Figure 1a are green stars, representing new $50\text{Na}_2\text{CO}_3$ - $50\text{K}_2\text{CO}_3$ data from this study (see Results), measured using the same equipment as described by Di Genova et al. (2016). This data set covers a larger temperature range, and so has a better-defined slope (green dotted line). The higher pressure Na_2CO_3 data of Stagno et al. (2018) in Figure 1a perhaps illustrates the challenge of performing accurate high-pressure measurements, and it remains unclear whether they define any systematic effect of pressure. Also included in Figure 1a are the data from Kim et al. (2015) for a $22\text{Li}_2\text{CO}_3$ - $33\text{Na}_2\text{CO}_3$ - $45\text{K}_2\text{CO}_3$ composition (purple stars). This eutectic in the Li_2CO_3 -bearing ternary system allows an even greater temperature range in measured viscosities. With such a large temperature range considered, some curvature clearly becomes evident, indicating a non-Arrhenian temperature dependence and raising questions regarding the validity of a linear fit to the other data.

Figure 1b contains a much more diverse range of mainly mixed carbonate compositions. Many involve alkaline-earth

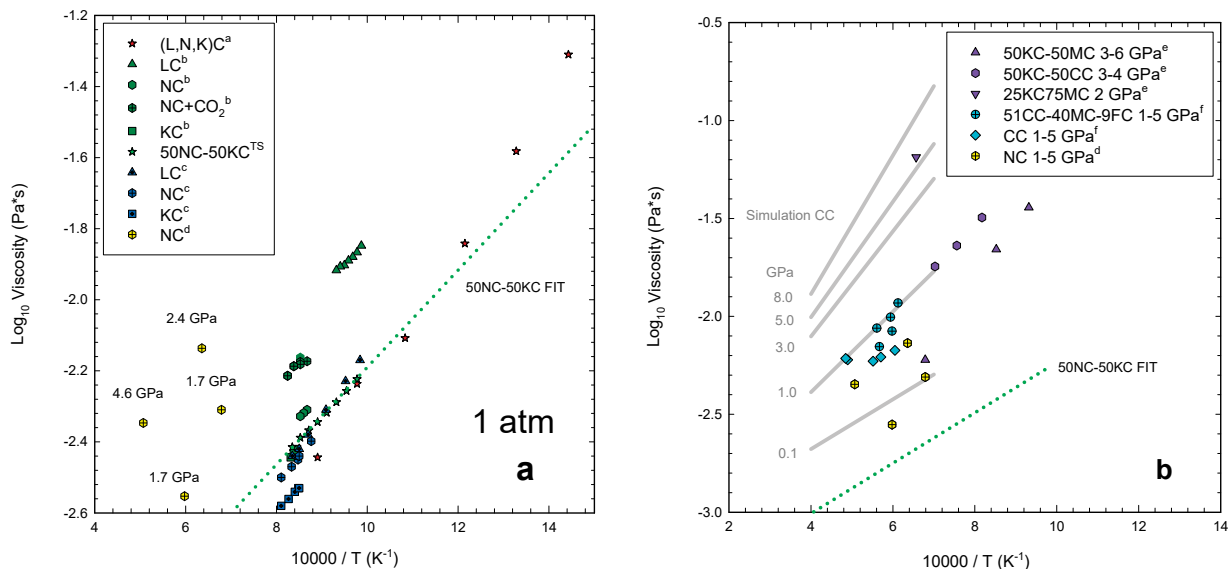


FIGURE 1. Previously measured viscosity data for (a) alkali-carbonates at atmospheric pressure (unless labeled) and (b) high-pressure experiments on alkali-earth and alkali carbonates (pressures indicated). The yellow hexagons for high-pressure NC data are also reproduced from (a). Also included in (a) are new $50\text{Na}_2\text{CO}_3$ - $50\text{K}_2\text{CO}_3$ data from the results of this study. Note, in this figure and the text, molar amounts of carbonate are expressed in the form: LC = Li_2CO_3 ; NC = Na_2CO_3 ; KC = K_2CO_3 ; MC = MgCO_3 ; CC = CaCO_3 ; FC = FeCO_3 ; except (Li,N,K)C = $22\text{Li}_2\text{CO}_3$ - $33\text{Na}_2\text{CO}_3$ - $45\text{K}_2\text{CO}_3$. The error is less than symbol size for the 1 atm measurements, the errors for the high pressure are hard to access. Data from: ^a Kim et al. (2015); ^b Di Genova et al. (2016); ^c Sato et al. (1999); ^{TS} This study; ^d Stagno et al. (2018); ^e Dobson et al. (1996); ^f Kono et al. (2014). The green dotted line in **a** is an Arrhenian fit through the $50\text{Na}_2\text{CO}_3$ - $50\text{K}_2\text{CO}_3$ data and reproduced in **b** for comparison. Simulation data for CC are taken from Vuilleumier et al. (2014), gray lines, at pressure indicated.

cations and therefore require pressure to ensure congruent melting. It is difficult to untangle the effect of composition from that of pressure, but the Dobson et al. (1996) study appears to include a range of data points on single lines for two compositional data sets covering a range of pressures from 2.5 to 5.5 GPa. These two lines generally bracket the different compositions of Kono et al. (2014), which cover an even larger pressure range from 0.9 to 5.3 GPa. In terms of composition, the green dotted line is representative of the alkali carbonates at 1 atm, when transferred to Figure 1b and could indicate either a lower viscosity for the alkali carbonates or some pressure effect with respect to the other high-temperature data. The lower viscosity of high-pressure measurements for Na_2CO_3 (yellow hexagons) compared to other compositions, but above the 1 atm data (green dotted line), appear to suggest both effects may be operating. Note that the K_2CO_3 high-pressure (4.0 GPa) data point of Dobson et al. (1996) was subsequently discredited (Liu et al. 2007; and therefore are not included in Fig. 1b), again illustrating the challenges in measuring physical properties using high-pressure experiments (Kono et al. 2014; Stagno et al. 2018). All the other high-temperature data in Figure 1b indicate the effect of pressure is less than half a \log_{10} unit between 0.9 and 5.5 GPa. The measured data appears at odds with the simulations of Vuilleumier et al. (2014), Du et al. (2018), and Desmaele et al. (2019a), which suggest a clear and more pronounced pressure effect. The seminal CaCO_3 data of Vuilleumier et al. (2014) is included in Figure 1b as an example, although these simulations may have overestimated the pressure effect to some extent and the role of forces such as van der Waals interactions require further refinement for these ab initio calculations (Vuilleumier, personal communication).

The glass transition and viscosity of “fragile” melts

As an aid to resolving some of the issues described above, an extension of the temperature range for viscosity determinations of carbonate liquids is a prime experimental goal. Most commercial glasses involve liquids with “covalent” network-forming components such as silicate, aluminate, or borate, and when cooled their increase in viscosity hinders nucleation and results in a glass with a characteristic, calorimetric glass transition reflecting this kinetic arrest (Moynihan 2019). Glass formation is however not restricted to network-forming liquids (Tangeman et al. 2001; Dingwell et al. 2004; Kohara et al. 2011). Glasses can even be formed from organic liquids and metallic systems. Of possible relevance to this study are glasses formed in simple ionic molten salts such as sulfate (Förland and Weyl 1950; MacFarlane 1984) and nitrate systems (Van Uitert and Grodkiewicz 1971). For these ionic compositions, the temperature-dependence of viscosity, a vital parameter in glass-formation, rarely exhibits Arrhenian behavior. This departure from Arrhenius law behavior is at the heart of the concept of liquid “fragility,” a term introduced by Angell (1985) to describe and compare the viscosity-temperature relations of a variety of glass-forming liquids. The quantification of fragility has been provided by the model-independent, so-called melt fragility index m (Böhmer et al. 1993). This index describes the rate of viscosity change of a melt with temperature at T_g , defined as the temperature where the viscosity is equal to 10^{12} Pa·s. The exact mechanism is thought to be related to medium-range structural heterogeneity, with faster and slower

relaxing regions developing as liquids are supercooled. There are formal links to the changes in the structure of supercooled liquids via the Adam-Gibbs model of structural relaxation (Gibbs and Adam 1965; Angell et al. 2000a, 2000b). Viscosity measurements made close to the glass transition can be used to evaluate liquid fragility (Gottsmann et al. 2002).

The linear Arrhenius law for viscosity (η) is expressed as:

$$\log_{10}\eta = A + E_a/T \quad (1)$$

and has two parameters to be fitted, E_a the activation energy is considered as the energy barrier that must overcome for examples as bonds are broken allowing molecules to “flow” from one position to another, and A is a numerical constant.

Thus, although viscosity-temperature data such as those in Figure 1 are commonly approximated over limited temperature ranges to an Arrhenian fit, it has long been known that for many materials the value of E_a changes with temperature yielding a non-Arrhenian curvature on a reciprocal absolute (Arrhenian) plot (Angell 1985; Böhmer et al. 1993). This is particularly evident as data are added from lower (supercooled) temperatures. One method of fitting such curvature is using the Vogel-Fulcher-Tammann equation (Vogel 1921; Fulcher 1925; Rault 2000) equation of the form:

$$\log_{10}\eta = A + B/[T(K) - C] \quad (2)$$

and B defined as: $B = (E_a \times 2.303)/R$ with R denoting the gas constant. This has the potential to reconcile a steep reciprocal temperature-dependence of low-temperature viscosity data with a lower reciprocal temperature dependence of high-temperature viscosity data and give the expected intersection of a \log_{10} value near -4 (in Pa·s) at infinite temperature.

Carbonate glasses

At the accessible quench rates of most experimental equipment (hundreds to thousands of K/s), carbonate melts rarely survive undercooling sufficient to produce glasses. As a result, direct investigation of their physico-chemical properties in the supercooled regime is currently limited to just the few known systems where glasses can be readily formed, MgCO_3 - K_2CO_3 (Eitel and Skaliks 1929; Datta et al. 1964; Ragone 1966; Genge et al. 1995) and $\text{La}(\text{OH})_3$ - $\text{Ca}(\text{OH})_2$ - CaCO_3 - CaF_2 - BaSO_4 (Jones and Wyllie 1983; Genge et al. 1995). Eitel and Skaliks (1929) were apparently the first to report a carbonate glass, quenched from $\sim 50:50$ mol% MgCO_3 - K_2CO_3 melts at 0.12 GPa. They also observed rapid devitrification of the glasses on an hour-timescale when held at a temperature between 205–300 °C. This is a common response to crossing the glass transition within poorly glass-forming systems such as nitrates, sulfates and carbonates and even basaltic silicates (Böhmer et al. 1993; Angell et al. 2000a; Wilding et al. 2000; Nichols et al. 2009). This implies the presence of T_g in this region of temperature and that the glass transition temperature for $\text{K}_2\text{Mg}(\text{CO}_3)_2$ might be located near 200 °C. To the best of our knowledge, this estimate has not been confirmed or used in the intervening 90 years, although Datta et al. (1964) did return to the system and mapped the glass-forming region.

Here, we report the first quantitative determination of a glass

transition for a carbonate liquid. Specifically, we demonstrate the nature of the glass transition and viscosity of a mixed K_2CO_3 - $MgCO_3$ carbonate melt by performing scanning calorimetry and viscometry on samples of a supercooled carbonate phase. Using this low-temperature viscosity data combined with published higher temperature (high pressure) data as well as both classical and ab initio molecular dynamics simulation estimates, we determine whether a non-Arrhenian Vogel-Fulcher-Tammann (VFT) law fit is possible and quantifies the extent of fragility.

MATERIALS AND METHODS

Glass synthesis

Carbonate glass was prepared using a starting mixture of 55 mol% K_2CO_3 and 45 mol% $MgCO_3$ (subsequently referred to as $55K_2CO_3$ -45 $MgCO_3$) using a rapid quench, cold-seal pressure vessel at the University of Bristol. This composition is directly above the eutectic (at $\sim 460^\circ C$) on the binary join (Ragone 1966), and glasses can be formed easily at the quench rates achieved ($\sim 200 K/s$) at a pressure of 0.1 GPa. Reagent-grade K_2CO_3 ($>99.9\%$) was dried at $400^\circ C$. The $MgCO_3$ was in the form of a natural, optically clear, and inclusion-free magnesite crystal (Brumado, Brazil), and transmission FTIR was used on thin cleavage fragments to confirm that this material was virtually water free. The starting materials were ground together and loaded in 3.8 mm diameter, 20 mm long gold capsules, which were then welded shut and loaded into a Tuttle-type cold-seal pressure vessel with a rapid quench rod extension (Ihinger 1991). The experiments were run at $780^\circ C$, 0.1 GPa for ~ 10 – 15 h. and quenched ($>200 K/s$). The resulting glass was removed from the gold capsule mostly as a single solid slug, representing the central part of the quenched melt, with an outer section that tends to spall off. This was stored in a desiccator. A small section was immediately set in dental resin and polished using dry SiC paper. Attenuated total reflectance (ATR) infrared spectroscopy data collected on this and similar samples indicate that some water may be present (see Wilding et al. 2019b). This was also confirmed by 1H NMR on similar samples (Wilding et al. 2019b). Wilding et al. (2019b) suggest this water is most likely introduced during loading or because the powders were improperly dried (in the case of the ^{13}C -enriched NMR sample). A comparison with the IR spectra of Genge

et al. (1995) suggests our samples contain significantly less water although it is very difficult to quantify. There is no evidence to suggest that the water content of the glass changes over the course of at least 24 h as demonstrated by a time series of spectra published in Wilding et al. (2019b). However, over the course of several weeks, samples can deteriorate even when stored in a desiccator and change in appearance from a transparent, pristine glass to an opaque white powder. This particular sample was transferred in one piece from Bristol to Munich within a few days of production and broken to extract a fresh interior sample for the measurements. The degree of hydration is unlikely to change over the course of the subsequent calorimetry experiments.

In addition, a $50Na_2CO_3$ - $50K_2CO_3$ (molar) carbonate mix was produced from Merck high-purity carbonates ($Na_2CO_3 \geq 99.9\%$; $K_2CO_3 \geq 99.5\%$) to compare with the previously published end-members in Figure 1a, but over a larger temperature range than previous data sets to better define the slope on a $1/T$ plot.

Thermogravimetry, calorimetry, and viscometry

Combined thermogravimetric analysis (TGA) and differential scanning calorimetry (DSC) was performed using a Netzsch STA 449 C/3/G Jupiter simultaneous viscometry analyzer at LMU. A single, transparent chip of the carbonate glass, of about 10 mg, was heated up to $920^\circ C$ at a constant rate of 5 K/min in a Pt-crucible under a purging, high-purity Argon atmosphere (30 mL/min; see Fig. 2). The temperature calibration was based on the melting points of indium, zinc, Ba-carbonate, and gold. The measurements were corrected for thermal drift. Differential Scanning Calorimetry measurements at greater sensitivity were made using a Netzsch DSC 404 C/3/F Pegasus calorimeter. This also involved a chip of carbonate glass (40 mg), placed in a platinum crucible and heated with constant rates of 5, 10, and 15 K/min up to a temperature of $250^\circ C$ under a high-purity Argon atmosphere (30 mL/min; see Fig. 3). The sample remained transparent until the end of the heating cycles. The melting points of indium, zinc, barium carbonate, and gold were also used to calibrate temperature for this instrument.

In addition, one shear viscosity measurement has been performed at $230^\circ C$ using the micro-penetration method under a purging, high-purity argon atmosphere (30 mL/min). For this measurement, the sample was held for 15 min at this dwell temperature prior to the initiation of indentation to establish thermal equilibration. A hemispherical iridium-indenter was used with a force of 1 N into the sample, and the penetration depth was monitored with time. The corresponding viscosity and error were calculated (Hess et al. 1995) and are tabulated in Table 1. Optical inspection after the measurement revealed a surficial tarnishing of the sample below the indenter.

The viscosity value was immediately taken after the mechanical relaxation of the measurement setup (some seconds) and is assumed to be uncorrupted by crystallization effects.

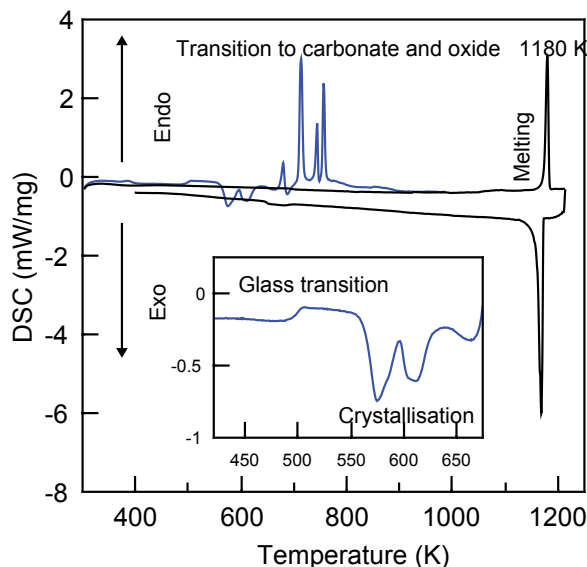


FIGURE 2. DSC/DTA measurements of a single $55K_2CO_3$ -45 $MgCO_3$ glass chip heated to $750^\circ C$. The onset of the glass transition is seen at about $225^\circ C$ (see inset). The relaxed glass is then devitrified shown by two exothermic crystallization peaks at ~ 300 and $\sim 340^\circ C$. On further heating the sample partly decomposes and forms a mixture of carbonates and oxides, which cannot be quenched to for a glass. The stable mixture melts at $900^\circ C$.

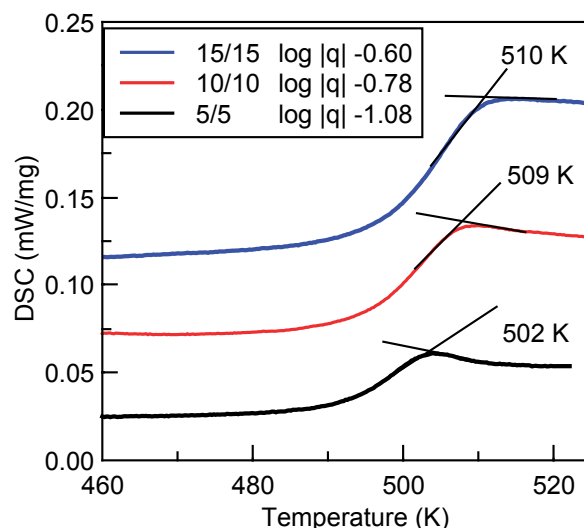


FIGURE 3. High-sensitivity DSC measurement of a 40 mg sample of $55K_2CO_3$ -45 $MgCO_3$ glass with a series of excursions across the glass transition with heating rate matched to prior cooling rate at the rates 5–15 K/min.

High-temperature $50\text{Na}_2\text{CO}_3\text{-}50\text{K}_2\text{CO}_3$ viscosity measurements were made using an adapted commercially available concentric cylinder rheometer (see Di Genova et al. 2016) equipped with a graphite furnace and featuring an air-bearing-supported synchronous motor and a specially designed Pt-Au concentric cylinder crucible and spindle assembly. With this adaptation, high-accuracy viscosity measurements of highly fluid melts can be achieved at high temperatures, up to 1273 K, and at extremely low torques. This allows accurate viscosity measurements as low as $10^{-3.5}$ Pa·s (and up to $10^{3.5}$ Pa·s at shear rates up to 10^2 s $^{-1}$). The apparatus was calibrated with distilled water, silicone oils, and the DGG-1 standard glass (see Di Genova et al. 2016). Super-liquidus $50\text{Na}_2\text{CO}_3\text{-}50\text{K}_2\text{CO}_3$ melt was measured from 1023 to 1198 K at a shear rate of 20 s $^{-1}$ (see Table 2).

First-principle (ab initio) molecular dynamics

The ab initio MD simulations for the $55\text{K}_2\text{CO}_3\text{-}45\text{MgCO}_3$ melt composition were performed using the Vienna Ab Initio Software Package (VASP) (Kresse and Furthmüller 1996a, 1996b). The electronic interactions described by projector-augmented wave (PAW) pseudopotentials (Blöchl 1994; Joubert 1999) were computed at the Brillouin zone Γ -point only with an energy cut-off value of 550 eV and the Perdew-Burke-Ernzerhof (PBE) formulation of the generalized gradient approximation (GGA) exchange correlation functional (Perdew et al. 1996). Molecular dynamics trajectories were computed in the canonical (NVT) ensemble with periodic boundary conditions and a Nosé thermostat (Nosé 1984).

The system was simulated using a randomly generated cubic cell of $N = 222$ atoms (44 K, 18 Mg, 40 C, 120 O) with initial closest approaches defined from the lowest crystallographic interatomic bond lengths. The starting configuration was super-heated to 10000 K for 2 ps, cooled isochorically to 2500 K over 4 ps, and equilibrated at final temperatures $T = 2500, 2100, 1800, 1500,$ and 1100 K for 30 ps. The final 25 ps of the equilibrated trajectories were taken for comput-

ing melt structure and properties. To mitigate for the under-binding of chemical bonds inherent to the GGA pseudopotential, we constrained the melt simulation cell volume, V , at each T to experimentally derived values at 1 atm, as calculated following Liu and Lange (2003). Our simulations suggest that Mg is dominantly in fivefold coordination, so a molar volume of 36.9 cm 3 /mol was used which is halfway between the values suggested for fourfold- and sixfold-coordinated Mg by Hurt and Lange (2019). The calculated density trend is only slightly lower than the ambient Dobson et al. (1996) measurements for $50\text{K}_2\text{CO}_3\text{-}50\text{MgCO}_3$ melt (2.1945 vs. 2.2621 at 723 K and 2.1439 vs. 2.2522 at 837 K), but at 2.3318 we nearly match the value of 2.325 measured for the glass (which we take as the melt density at a T_g of ~ 500 K). However, it should be noted that we have used the thermal expansivities of CaCO_3 . Although this appears to be applicable to all alkaline earth carbonates (Hurt and Lange 2019), it is extrapolated outside the calibrated range for the high temperature of the simulations and assumes a temperature-independent thermal expansivity, which is not an accurate assumption for liquids (e.g., Knoche et al. 1992; Dingwell et al. 1993). For the simulations used in this study (including data from Wilson et al. 2018; Wilding et al. 2019a) the derived diffusion data are converted to a viscosity using the Stokes-Einstein relationship either for the alkali atoms or the average of alkali and carbon atoms.

RESULTS

DSC and DTA glass transition determination

The results of differential thermal and thermogravimetric analysis (DTA-TGA) and differential scanning calorimetry (DSC) are shown in Figures 2 and 3 and tabulated in Table 1 for the $55\text{K}_2\text{CO}_3\text{-}45\text{MgCO}_3$ glass. The DTA analysis (Fig. 2) shows clearly the glass transition onset at ~ 220 °C (493 K). There is a small peak at 120 °C, which we interpret as the loss of surface water from these samples. Above 260 °C (533 K) the DTA curves show a series of exothermic peaks, which result from crystallization, followed by phase transitions (above 400 °C) and finally at higher temperatures, endothermic peaks that represent a solid-state reaction and partial decarbonation resulting in a mixture of carbonates and oxides. The onset of melting occurs at 900 °C (1173 K). On cooling, crystallization occurs at the same temperature, and thus liquidus and solidus temperatures are consistent. This liquidus temperature for the $55\text{K}_2\text{CO}_3\text{-}45\text{MgCO}_3$ composition is much higher than the 500 °C expected from the 0.1 GPa phase diagram of Ragone (1966). The reported eutectic in the

TABLE 1. $\text{K}_2\text{CO}_3\text{-MgCO}_3$ melt viscosity data from differential scanning calorimetry (DSC), micro-penetration viscometry (MP), and falling sphere viscometry data (FS) used for an unweighted VFT fitting

Method	T (°C)	Quench rate log q (K/s)	Viscosity log (Pa·s)	Error	Pressure
DSC ^a	237	-0.60	8.55	0.09	1 atm
DSC ^a	234	-0.78	8.73	0.09	1 atm
VISC-MP	230		8.95	0.06	1 atm
DSC ^a	229	-1.08	9.03	0.09	1 atm
VISC-FS ^b	800		-1.44	0.43	3 GPa
VISC-FS ^b	900		-1.66	0.43	3 GPa
VISC-FS ^b	1200		-2.22	0.43	5 GPa

^a Using a shift factor of 7.95; error in T converted in error in viscosity.

^b From Dobson et al. (1996).

TABLE 2. Diffusion coefficients obtained from simulations and used to derive viscosities

T (K)	Potassium			Carbon			Average	
	log D (cm 2 /s)	log η (Pa·s)	Error	log D (cm 2 /s)	log $_{10}$ (Pa·s)	Error	log $_{10}$ (Pa·s)	Error
$55\text{K}_2\text{CO}_3\text{-}45\text{MgCO}_3$								
1500 ^a	-4.875	-2.789	-0.244	-4.718	-2.308	-0.115	-2.548	-0.127
1800 ^a	-3.998	-2.949	-0.200	-4.407	-2.540	-0.127	-2.744	-0.137
2100 ^a	-3.857	-3.023	-0.193	-4.162	-2.718	-0.136	-2.870	-0.144
2500 ^a	-3.538	-3.267	-0.177	-3.900	-2.904	-0.145	-3.085	-0.154
1850 ^b	-4	-2.935	-0.200	-	-	-	-	-
Na_2CO_3								
T (K)	Sodium			Carbon			Average	
	log D (cm 2 /s)	log (Pa·s)	Error	log D (cm 2 /s)	log $_{10}$ (Pa·s)	Error	log $_{10}$ (Pa·s)	Error
800	-5.295	-2.034	-0.477	-5.894	-1.435	-0.530	-1.735	-0.503
900	-4.896	-2.382	-0.441	-5.335	-1.943	-0.480	-2.162	-0.460
1000	-4.635	-2.597	-0.324	-5.086	-2.146	-0.356	-2.372	-0.340
1100	-4.461	-2.730	-0.223	-4.958	-2.233	-0.248	-2.481	-0.235
1200	-4.353	-2.800	-0.174	-4.823	-2.330	-0.193	-2.565	-0.184
1300	-4.186	-2.932	-0.126	-4.668	-2.451	-0.140	-2.691	-0.133
1400	-4.089	-2.998	-0.123	-4.543	-2.543	-0.136	-2.770	-0.129
1500	-4.011	-3.045	-0.120	-4.478	-2.578	-0.134	-2.812	-0.127
1600	-3.958	-3.070	-0.079	-4.434	-2.594	-0.089	-2.832	-0.084
1750	-3.835	-3.154	-0.038	-4.347	-2.642	-0.043	-2.898	-0.041
2000	-3.710	-3.221	-0.037	-4.132	-2.800	-0.041	-3.010	-0.039
2500	-3.528	-3.306	-0.035	-3.971	-2.864	-0.040	-3.085	-0.037

^a Values derived from ab initio calculations.

^b Values derived from The classical simulations presented in Wilding et al. (2019a) where only the K diffusivity is provided.

^c Values derived from Wilson et al. (2018) for a favored "q" value of 2.28 (see Online Materials⁵).

binary system ($57\text{K}_2\text{CO}_3\text{--}43\text{MgCO}_3$ at 0.1 GPa) is at 460°C , although the liquidus rises very steeply with composition. This may suggest a change in composition and the loss of CO_2 at ambient pressure consistent with the observation of Eitel and Skaliks (1929) that high pressure is required to ensure melting of K_2CO_3 and MgCO_3 constituents without decomposition, but we note that any such effect is post- T_g determination.

The results of the high-sensitivity DSC measurements are shown in Figure 3. The as-quenched glass was heated through the glass transition into the supercooled liquid regime at 250°C (523 K) where the liquid is fully relaxed. The glass sample was then subjected to a series of thermal cycles comprising excursions across the glass transition at different heating rates, with the heating rate matched to the prior cooling rate (i.e., for example, a heating rate of 5 K/min is matched with a previous cooling rate of 5 K/min) (Easteal et al. 1977). With this approach of matching cooling and heating rates, the so-called onset of the calorimetric glass transition corresponds to the fictive temperature (Moynihan 1993, 2019; Yue et al. 2004) determined by the enthalpy-matching method (Moynihan et al. 1976; Yue 2008). As the sample is heated at rates of 5, 10, and 15 K/min, the temperature of the glass transition (taken as the peak position corresponding to the heat flow peak overshoot, hereafter referred to as T_{peak}) shifts systematically with matched heating/cooling rate ($|q|$) from 229 to $237 \pm 1^\circ\text{C}$ (502–510 K) for 5 to 15 K/min. The combined thermo-gravimetry (TG) and calorimetry (DSC) measurements demonstrate the thermal stability of the glass sample; the glass transition is clearly identified at $229 \pm 1^\circ\text{C}$ (for a cooling rate of 15 K/min), which is consistent with the original study of Eitel and Skaliks (1929) based on rapid devitrification of the glass between $200\text{--}300^\circ\text{C}$.

Shift factor

The shift factor K (here K_{peak}) (Scherer 2006; Stevenson et al. 1995; Gottsmann et al. 2002; Yue et al. 2004; Al-Mukadam et al. 2020) can be derived from the DSC measurements (Fig. 3) by matching the characteristic glass transition temperature T_{peak} for a given cooling/heating (q , K/s) cycle to the temperature of the viscosity measurement:

$$K_{\text{peak}} = \log_{10}\eta(T_{\text{peak}}) + \log_{10}|q| \quad (3)$$

The value (7.95) obtained at cooling/heating rates of 15 K/min (where the temperatures overlap with the accuracy of the measurements) is then used for the other cooling/heating cycles:

$$\log_{10}\eta(T_{\text{peak}}) = K_{\text{peak}} - \log_{10}|q| \quad (4)$$

to calculate the viscosity for the $55\text{K}_2\text{CO}_3\text{--}45\text{MgCO}_3$ liquid (Table 1) ranging from $\log_{10} 9.03 \pm 0.09$ Pa·s at 229°C to $\log_{10} 8.55$ Pa·s ± 0.09 at 237°C (error in temperature was converted to error in viscosity). We note that this shift factor is lower than that observed for silicate melts but is generally consistent with high compressibility as expected for carbonate melts.

A viscosity–temperature relationship for carbonate melts

For the $55\text{K}_2\text{CO}_3\text{--}45\text{MgCO}_3$ sample, the three viscosities derived using DSC measurements and the shift factor together

with the one data point from the micro-penetration measurement are plotted in Figure 4. These low-temperature data can be fitted to a single Arrhenian trend, but the slope greatly exceeds that of an Arrhenian fit solely through the high-temperature $50\text{K}_2\text{CO}_3\text{--}50\text{MgCO}_3$ data of Dobson et al. (1996) or Sifré et al. (2015), or the trends of simulation data plotted in Figure 4. It is clear that both Arrhenian subsets of data exhibit slopes that are Arrhenian only as artifacts of the very restricted temperature ranges of the individual data sets. Taken together, the data describe a strongly non-Arrhenian temperature-dependence of viscosity. An unweighted Vogel-Fulcher-Tammann (VFT) fit through both data sets is shown in Figure 4. The resultant fit using the Dobson et al. (1996) data demonstrates the “fragility” of this system. At high temperatures, this fit also agrees well with the $50\text{K}_2\text{CO}_3\text{--}50\text{MgCO}_3$ data of Sifré et al. (2015), who measured the electrical conductivity and demonstrated how this high-temperature data could be converted to a viscosity. It must be borne in mind, however, that both Dobson et al. (1996) and Sifré et al. (2015) data are at high pressure (3–6 GPa). As the magnitude of any pressure effect remains controversial and it is not possible to conduct high-temperature viscosity measurements at 1 atm to directly complement the DSC data, we have further extended (for further comparison) the $55\text{K}_2\text{CO}_3\text{--}45\text{MgCO}_3$ data set using ab initio simulation data in Table 2. These 1 atm results are included in Figure 4, where they lie close to the Dobson et al. (1996) high-pressure data. In fact, our simulations indicate that from 1 atm to 3 GPa, there is less than half \log_{10} unit increase in viscosity. Also included in Figure 4 is an additional simulation data point for “ambient” pressure $55\text{K}_2\text{CO}_3\text{--}45\text{MgCO}_3$ melt derived from the classical simulations of Wilding et al. (2019a, 2019b), which are consistent with high-energy XRD data used to elucidate the $55\text{K}_2\text{CO}_3\text{--}45\text{MgCO}_3$ glass structure.

When evaluating the reliability of the Dobson et al. (1996) $50\text{K}_2\text{CO}_3\text{--}50\text{MgCO}_3$ viscosities, Kono et al. (2015) implied that they should lie $0.5 \log_{10}$ unit higher to match the $50\text{K}_2\text{CO}_3\text{--}$

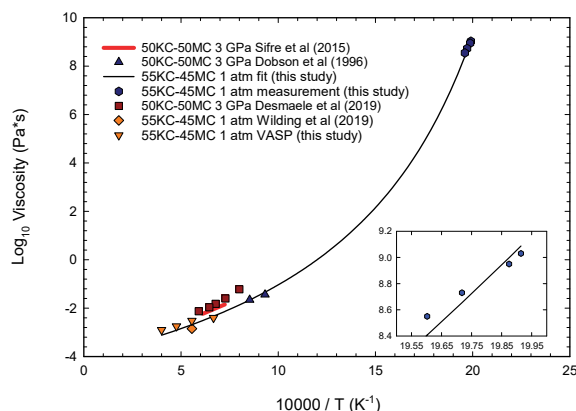


FIGURE 4. Viscosity curve for $55\text{K}_2\text{CO}_3\text{--}45\text{MgCO}_3$ composition liquid obtained by VFT fit to the low-temperature viscosity data from this study, and the $55\text{K}_2\text{CO}_3\text{--}45\text{MgCO}_3$ liquid viscosity data at 3–5 GPa from Dobson et al. (1996). The fit is bracketed by the simulations of Wilding et al. (2019a, 2019b) and the VASP data (average diffusion coefficients) from this study, both at 1 atm. For comparison, the Sifré et al. (2015) conductivity data for a similar composition at 3 GPa, has been converted to a viscosity. Also shown are the simulations of Desmaele et al. (2019a).

50CaCO₃ Dobson et al. (1996) data as no compositional effect was expected. Desmaele et al. (2019a) also concluded that the compositions should have similar viscosity but also indicated that the effect of pressure would reduce this value by a log₁₀ unit at 1 atm. Given all these unresolved discrepancies, we have chosen to fit to the Dobson et al. (1996) 50K₂CO₃–50MgCO₃ data accepting they are possibly too high and that a reduction in pressure brings them down and closer to our 1 atm simulated data for 55K₂CO₃–45MgCO₃. Regardless of which high-temperature data set is used, it is clear the 55K₂CO₃–45MgCO₃ melt is highly fragile. The VFT fitting also indicates a value between –3 and –4 log₁₀ (in Pa·s) at an infinite temperature consistent with other theoretical and statistical estimates (Angell et al. 1989). A calculated VFT for Na₂CO₃ is also illustrated for comparison in Figure 5. This represents the viscosity obtained from the diffusion data obtained from the classical MD simulations of Wilson et al. (2018), which are tabulated in Table 2. The “q” value, the degree of charge separation across the carbonate anion (explained in Online Materials¹) is 2.28, and the simulated diffraction pattern at this value gives the best fit to the data obtained from high-energy XRD measurements on molten Na₂CO₃. The diffusion (and viscosity) data obtained at this value of charge separation shows fragile (non-Arrhenian) behavior, correlated with the temperature-dependent abundance of CO₃²⁻ rings and other complexes. Using this value of charge separation gives the best VFT fit to the experimental Na₂CO₃ viscosity data of Di Genova et al. (2016) in Figure 5 and illustrates the robustness of this simulation methodology.

Figure 5 also contains our new viscosity measurements for 50Na₂CO₃–50K₂CO₃, listed in Table 3. This composition is consistent with the Di Genova et al. (2016) data set plotting between viscosity data curves for Na₂CO₃ and K₂CO₃ when measured under an argon atmosphere (see Fig. 1a). In the context of comparing to the Na₂CO₃ VFT curve, this data has the advantage of a larger temperature range than the Na₂CO₃ measurements. The 50Na₂CO₃–50K₂CO₃ binary viscosity data set can be fitted with

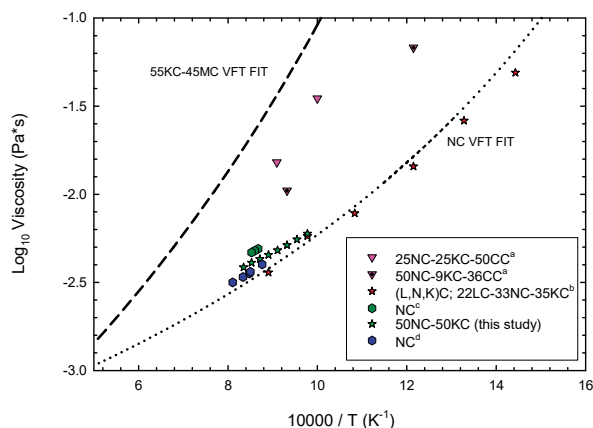


FIGURE 5. The sodium carbonate VFT fit has been derived from the simulations of Wilson et al. (2018), but with selected parameters to best fit the sodium carbonate data of Di Genova et al. (2016). Other published data for synthetic alkali carbonate mixes ranging from pure alkalis, to variable amounts of added calcium carbonate. Data from: ^a Desmaele et al. (2019b); ^b Kim et al. (2015); ^c Di Genova et al. (2016); ^d Sato et al. (1999).

TABLE 3. High-temperature viscometry data for synthetic alkali carbonate melts

T (°C)	10000/T (K ⁻¹)	η (Pa·s)	log η (Pa·s) ^a	Shear rate (s ⁻¹)
50Na₂CO₃–50K₂CO₃				
750	9.775	0.00598	-2.22	20
775	9.542	0.00554	-2.26	20
800	9.320	0.00515	-2.29	20
825	9.107	0.00481	-2.32	20
850	8.905	0.00453	-2.34	20
875	8.711	0.00429	-2.37	20
900	8.525	0.00409	-2.39	20
925	8.347	0.00385	-2.41	20

^a Error is ±0.01 log (Pa·s).

a linear trend within error, but a slight positive curvature would also be permitted. The curved trend for the 22Li₂CO₃–33Na₂CO₃–45K₂CO₃ eutectic composition of Kim et al. (2015), as noted in Figure 1, is reproduced in Figure 5 and is also consistent with our Na₂CO₃ VFT curve.

The other synthetic composition data shown in Figure 5 are simulations performed by Desmaele et al. (2019b) that reveal the effect of adding calcium to the sodium-potassium system. Starting from the 50Na₂CO₃–50K₂CO₃ composition of this study, there is a clear increase in viscosity with the addition of CaCO₃. Although Desmaele et al. (2019b) provide only two data points, they are consistent with a decrease in fragility with CaCO₃ addition.

DISCUSSION

Carbonate melt structure

The structure of levitated alkali carbonate liquids has been studied directly using high-energy X-ray diffraction (Wilding et al. 2016; Wilson et al. 2018). These diffraction data have been combined with classical molecular dynamic simulations and used to evaluate the changes in the liquid structure with temperature and accordingly the carbonate liquid fragility. Central to the simulation methodology is the flexibility of the carbonate anion geometry. Spectroscopic studies of the K₂CO₃–MgCO₃ glass (Sharma and Simons 1980; Genge et al. 1995; Wilding et al. 2019a, 2019b) have suggested the presence of two structurally distinct populations of carbonate anion, one of which is more distorted, and it is this distortion of the carbonate that has been used as a basis for the molecular dynamics simulation of the alkali carbonate liquids. In the simulation of Na₂CO₃, flexibility is imposed by employing springs between the O–O and C–O pairs in the anion, and the stiffness of these springs is constrained by comparing the liquid diffraction patterns at high and low values of scattering vector with the simulated liquid structure, the inter- and intra-molecular contributions, respectively. Once constrained, the simulated liquid structure can be explored as a function of temperature. The flexibility of the molecular carbonate anion allows the central carbon atom to be drawn out of the triangular plane and the anion becomes polarized. One consequence of this is that there is the development of a secondary length scale and the development of carbonate chains and other carbonate complexes, the extent of which is strongly temperature dependent. In a more recent study (Wilson et al. 2018), the fluctuation of charge across the molecular anion was introduced into the simulation to further explore the dynamics of sodium carbonate liquids and demonstrates a correlation between the development of carbonate complexes and liquid fragility, with

the connectivity of these emergent structures dependent on the mean charge separation (see Online Materials¹).

This modeling approach, with the flexibility of the molecular anion, has also been applied to the K_2CO_3 – $MgCO_3$ system where the simulations are used to identify the pressure-dependent changes in structure of the same $55K_2CO_3$ – $45MgCO_3$ glass studied here. At ambient pressure, there is no evidence for formation of carbonate chains or other complex structures in the $55K_2CO_3$ – $45MgCO_3$ carbonate liquids. However, as pressure is increased, there is the development of a carbonate network associated with an increase in the mean coordination number of the carbon with the development of a CO_{3+n} configuration (Wilding et al. 2019a). The response to pressure in these liquids again reflects the flexibility of the carbonate and the complex interaction between the oxygen atoms in the CO_3^{2-} anion and their strong electrostatic interaction with potassium cations. The ambient pressure glass does not show the development of this network, but ^{13}C NMR confirms a distorted carbonate anion (Wilding et al. 2019b), while infrared spectroscopy confirms the presence of two structurally distinct populations of carbonate anions identified in earlier studies. In fact, the simulation of the liquids suggests different degrees of flexibility of the carbonate anion rather than two distinct populations with the stronger interactions with Mg^{2+} and K^+ cations associated with the more distorted carbonate. Nonetheless, the simulation of the K_2CO_3 – $MgCO_3$ liquid shows distorted carbonate with magnesium and potassium cations occupying irregular channels and with both types of cations adopting a network-forming role by bridging isolated carbonate anions (Wilding et al. 2019b). It has been suggested that glass formation in sulfate and nitrate systems also requires the presence of two different cations with different field strengths and different degrees of polarizability (Förland and Weyl 1950; van Uitert and Grodkiewicz 1971; MacFarlane 1984; Wilding et al. 2017).

The ab initio molecular dynamics simulations that form part of this study can be used to evaluate the changes in the ambient pressure liquid structure as a function of temperature. As expected, there is no formation of a Na_2CO_3 style carbonate network in $55K_2CO_3$ – $45MgCO_3$. However, the main changes in structure occur in the local environment surrounding the K^+ cations. There is an increase in the mean K–O coordination number, which increases as the temperature is decreased, but no change in the average C–O coordination at ambient pressure. The distortion in the local environments for potassium is shown in the changes in the partial contributions to the pair distribution functions for K–O and K–K (Online Materials¹). The coordination environments for both potassium and magnesium differ significantly from those in the equivalent crystalline phase, illustrated in a snapshot from the ab initio simulation in Figure 6.

As noted above, the K_2CO_3 – $MgCO_3$ composition is not a naturally occurring carbonate liquid. However, this and related studies show that combining experimentally derived structures and structure-related properties with classic and ab initio simulation provides insight into the viscosity-temperature relations of mixed carbonate liquids and that the same modeling approach can be extended to naturally occurring systems. In contrast to the alkali carbonates, there is no evidence for the formation of a carbonate network in the K_2CO_3 – $MgCO_3$ liquids. However,

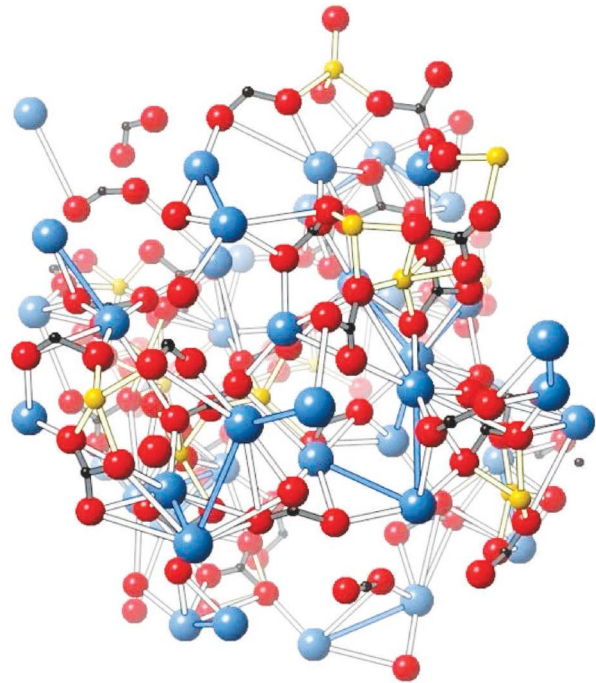


FIGURE 6. A snapshot of the high-temperature liquid configuration, carbon atoms are shown in black, oxygen atoms red, potassium atoms blue, and magnesium atoms yellow, obtained directly from the ab initio MD (VASP) simulation trajectories for liquid $55K_2CO_3$ – $45MgCO_3$ at 2500 K.

the liquid dynamics still reflect the underlying flexibility of the carbonate anion.

The fragility of carbonate melts

The carbonate melt viscosities are compared in reciprocal absolute temperature (Arrhenian) space with other geologically relevant liquids in Figure 7 using the data in Table 4. This comparison confirms that under similar conditions, the carbonate liquids have very low viscosity and are potentially very mobile, at least at the

TABLE 4. Fit parameters describing the temperature dependence of the viscosity (VFT), the glass transition temperature T_{12} , the activation energy $E_a(T_{12})$ and the fragility index (m) for carbonates in this study and selected silicate liquids of geological relevance

Composition	A log (Pa·s)	B (K^{-1})	C (K)	T_{12} (K)	$E_a(T_{12})$ kJ/mol	Fragility index (m)
Haplo-rhyolite ^a	–6.219	15950	232.2	1108	489	23
Phonolite ^b	–4.550	10261	263.8	884	399	24
Trachyte ^b	–4.550	10449	303.7	935	439	25
SiO ₂ ^c	–4.167	15336	508.5	1457	693	25
Basalt ^b	–4.550	6101	567.0	936	753	42
$55K_2CO_3$ – $45MgCO_3$	–4.010	1914	356.0	476	580	64
Peridotite ^d	–4.310	3703	761.7	989	1345	71
Na_2CO_3	–3.470	832	329.0	383	807	110
CKN ^e	–3.602	798	324.4	376	824	115

Notes: Glass transition temperature T_{12} at \log_{10} 12 Pa·s, activation energy E_a at T_{12} derived from VFT parameter.

^a Data from Dorfman et al. (1996).

^b Data from Giordano et al. (2009).

^c Data from Hetherington et al. (1964) and Hofmaier and Urbain (1968).

^d Data from Dingwell et al. (2004).

^e Data from Tweer et al. (1971) and Weiler et al. (1969).

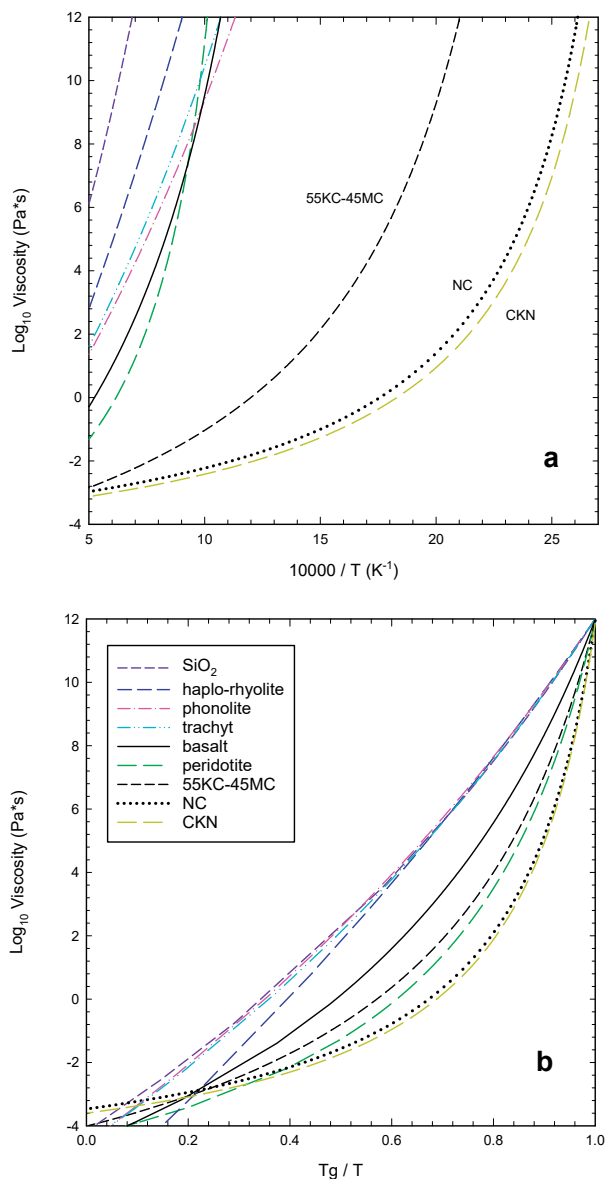


FIGURE 7. (a) Viscosity vs. temperature in an Arrhenian plot. (b) Viscosity curves standardized to their glass transition (T_{12}) to give a fragility (Angell) plot of liquids of geological relevance, and also for the archetypal fragile liquids $40\text{CaNO}_3\text{-}60\text{K}_2\text{NO}_3$ (CKN). The VFT curves from this study are included and as expected the carbonates are significantly more fragile than the silicates.

ambient pressures measured in this study.

The VFT fit is a powerful tool in enabling the extrapolation of the temperature–viscosity relationship to higher temperatures and thereby constraining the pre-exponential term in the temperature-dependent viscosity equation (cf. Russell et al. 2003). As previously noted, the pre-exponential term or viscosity limit at infinite temperature lies just above 10^{-4} Pa·s, a value consistent with literature data for other simple molecular liquid classes (oxides, halides, silicates, etc.). In Figure 7a, (see Table 4), the viscosities of $55\text{K}_2\text{CO}_3\text{-}45\text{MgCO}_3$ and Na_2CO_3 liquids are compared with the viscosity of several silicates as well as $40\text{CaNO}_3\text{-}60\text{K}_2\text{NO}_3$ (CKN),

generally considered to be an archetypal fragile liquid. In Figure 7b, these are compared in an Angell plot (Böhmer et al. 1993; Angell and Moyniha 2000) with the temperature normalized to T_g , and the liquids show progressive departure from the Arrhenius behavior of “strong liquids” such as the network-forming liquid SiO_2 , seen as a series of curves of increasing fragility. The different degrees of fragility reflect differences in the temperature-dependence of liquid structure through their relative contributions to the configurational entropy (Richet 1984). The temperature-dependent structural elements might be locally favored structures, dynamic heterogeneities, or density fluctuations within the supercooled liquid state.

IMPLICATIONS

It will be apparent that the fragility of the carbonate liquid and its high-temperature viscosity are very similar to those of a peridotite melt (Dingwell et al. 2004). Liquid peridotite is one of the most fragile silicate compositions ever measured and is extremely difficult to quench to a glass. Peridotite is an example of a “fully depolymerized” silicate melt, where the silicate network structure is broken into isolated units surrounded by metal cations (cf. Kohara et al. 2011). Peridotite and carbonate melts lie at higher fragility than all the other petrologically and volcanologically relevant silicate melts, including basalts (Giordano and Dingwell 2003), extremely peralkaline phonolites and pantellerites (Whittington et al. 2001; Di Genova et al. 2013), and water-rich calc-alkaline rhyolites (Hess and Dingwell 1996). Peridotite melt may have formed the magma ocean in early Earth history when carbonate content could also have been relatively high. In fact, at high enough pressures, there is a continuum from carbonate melt to “depolymerized” high- CO_2 silicate melt compositions (such as melilitites) generated during high-temperature carbonated mantle melting (e.g., Brey and Green 1976; Gudfinnsson and Presnall 2005). Initially, SiO_2 that is added to dilute the carbonate melt will remain as isolated “ SiO_4 ” units with little effect on the ionic structure and, therefore, viscosity. But as SiO_2 (and Al_2O_3) reaches 15–30 wt% these transitional melt compositions (Brooker et al. 2011) form new structures with two sub-networks, one consisting of regions with polymerized silicate structures and the other ionic carbonate. These may be precursors to silicate-carbonate immiscibility (Brooker et al. 2001; Morizet et al. 2017). The presence of two sub-networks at the molecular level could lead to a complex viscosity temperature dependence related to this medium-range structural heterogeneity, with the faster and slower relaxing regions that are often cited as a cause of fragility. However, the viscosity determinations of Morizet et al. (2017) and those inferred by the conductivity measurements of Sifré et al. (2014) suggest that various amounts of CO_2 in transitional or basaltic silicate melts and thus the proportion of the two sub-networks, has little effect on the viscosity, which remains similar to the CO_2 -free silicate composition. This is consistent with our observations here that all very high-temperature interactions between extremely fragile very low-silica silicate melts (e.g., peridotite, melilitite, kimberlite) and carbonatites will be interactions between two liquids of similar low viscosities.

The absolute values of the glass transition temperatures, together with the restricted range of glass-forming ability in carbonatite, means that the likelihood of encountering glassy behavior in natural magmatic systems is vanishingly small.

The more rapid increase in viscosity at lower temperatures is obviously more important in silicate systems, particularly for silica-rich eruptions where volatiles are being exsolved. Gas bubbles are unable to escape, instead building up internal pressure that results in explosive behavior and fragmentation of a supercooled melt (i.e., glass) as the viscosity approached some critical value (usually considered around 10^7 Pa·s; e.g., Namiki and Manga 2008). The stoichiometry of the carbonate components within carbonatite melts suggests that the main volatile component (CO_2) is not necessarily exsolved, at least in alkali-rich systems. Even if other volatiles are exsolved, the general low viscosities at eruptive temperatures (see Fig. 7a) will allow bubbles to escape through the melt more efficiently than in a silicate melt. The exception to this could be the apparently explosive alkaline-earth carbonatite volcanism that produced rounded lapilli melt droplets, preserved at the Kaiserstuhl volcanic complex (Keller 1989). These have an almost pure CaCO_3 composition, and the shape and internal structure suggest these are airborne quenched melt. Pure CaCO_3 should dissociate at pressures below 0.004 GPa, so how this composition could erupt molten droplets is still a mystery. This has prompted the usual idea that minor amounts of alkalis or fluorine allow the melt to exist at low pressure and these are subsequently leached away (Gittins and Jago 1991; Brooker and Kjarsgaard 2011). However, one could speculate that a rapid increase in viscosity and cooling within some “ CO_2 confining pressure” in the vent could combine to preserve a CaCO_3 melt as droplets. Zimanowski et al. (1986) have demonstrated droplet formation for $50\text{Na}_2\text{CO}_3$ – $50\text{K}_2\text{CO}_3$ and Oldoinyo Lengai carbonatites by the interaction of the melt with injected water. As Zimanowski et al. (1986) point out, these processes are perhaps also important for modeling explosive situations involving industrial molten salt cells where a full understanding of the physical processes becomes important as regards hazard mitigation.

Zimanowski et al. (1997) have indeed directly observed the fracturing of a high-temperature carbonate liquid upon interaction with external water. They effectively induced the glass transition in the carbonate liquid and recorded the results by high-speed video. These observations are entirely consistent with the observation here that a glass transition can be encountered in molten carbonates. With knowledge of the viscosity–temperature curve observed here, together with the effective temperature of the melt–water interaction in the experiments of Zimanowski et al. (1997), one should be able in principle to estimate the volume strain rates at the point of brittle failure of the carbonate liquid. Alternatively, if the thermal stresses are well-estimated, then one should be able to predict the effective temperature of the brittle failure-inducing melt–water interaction. That would have been impossible to achieve accurately with a degree of certainty by simply using extrapolations of super-liquidus viscosity–temperature relations.

A nonlinear rate change in viscosity is also an important parameter in understanding the nature of carbonatite lava flows, particularly the length and terminal velocity at Oldoinyo Lengai. The same applies to the calculations of Treiman and Schedl (1983), who calculated the carbonatite melt properties in magma chambers and their effect on turbulence and the rapid setting velocities of crystals and growth rates on chamber walls, with

implications also for the settling rate in lava flows (Norton and Pinkerton 1997).

The most widespread occurrence of carbonate melts is most likely deep in the Earth’s mantle. Dalton and Wood (1993) demonstrated that carbonatites generated by melting a depleted carbonated mantle source are almost alkali-free, ranging from 25MgCO_3 – 75CaCO_3 to 8MgCO_3 – 92CaCO_3 (with some minor FeCO_3), but sodium can reach $15\text{Na}_2\text{CO}_3$ for a fertile mantle source and subsequently be increased or decreased due to metasomatic wall–rock reactions. The range of compositions derived from subducted altered basalt (eclogite) in Thomson et al. (2016) is even more diverse, ranging to higher contents of iron- and alkalis (14 – 24FeCO_3 , 9 – 15MgCO_3 , 43 – 66CaCO_3 , 2 – $29\text{Na}_2\text{CO}_3$, 1 – $3\text{K}_2\text{CO}_3$). At these conditions, the viscosity can be reasonably well approximated by a linear temperature dependence trend. The possible compositional effect of Na_2CO_3 inferred from Figures 1b and 5 suggest this is an important component when considering the viscosity of mantle carbonatites, although these mantle melts are all produced at high temperatures (>1200 °C) and even 1 atm sodic melts would have viscosities within 0.5 \log_{10} units of the other compositions in Figure 1b. However, the hydrous “fertile pyrolite” composition of Wallace and Green (1988) produced an alkali-rich carbonatite melt ($\sim 5\text{K}_2\text{CO}_3$ – $33\text{Na}_2\text{CO}_3$ – 62CaCO_3) at temperatures between 930 and 1080 °C at 2.1 GPa. Wallace and Green (1988) suggest an even more alkali-rich carbonate melt may exist at even lower temperatures, perhaps forming before the water is released by hydrous silicate minerals. These low temperatures are realistic for the shallow lithosphere beneath the old continental crust, and this is getting into the temperature range where a linear fit based on the high-temperature data will become inaccurate, and the high fragility of the Na_2CO_3 component may become important (Fig. 5). This would have implications for modeling the transport properties of these melts to their surface expression or as metasomatizing agents.

ACKNOWLEDGMENTS AND FUNDING

We thank Fabrice Gaillard and Rodolphe Vuilleumier for fruitful suggestions that greatly improved the manuscript. R.A.B was funded by the NERC Thematic Grant consortium NE/M000419/1. J.W.E.D acknowledges support from NERC under Grant NE/P002951/1. D.B.D. acknowledges the support of ERC 2018 ADV Grant 834255 (EAVESDROP).

REFERENCES CITED

- Al-Mukadam, R., Di Genova, D., Bomhöft, H., and Deubener, J. (2020) High rate calorimetry derived viscosity of oxide melts prone to crystallization. *Journal of Non-Crystalline Solids*, 536, 119992.
- Angell, C.A. (1985) Strong and fragile liquids. *Relaxations in Complex Systems*. U.S. Department of Commerce National Technical Information Service, Springfield, Virginia, 3, 3–11.
- Angell, C.A., and Moynihan, C.T. (2000) Ideal and cooperative bond-lattice representations of excitations in glass-forming liquids: excitation profiles, fragilities, and phase transitions. *Metallurgical and Materials Transactions B*, 31, 587–596.
- Angell, C.A., Scamehorn, C.A., List, D.J., and Kieffer, J. (1989) Glass forming liquid oxides at the fragile limit of the viscosity-temperature relationship. From Proceedings of XV International Congress on Glasse, Leningrad.
- Angell, C.A., Moynihan, C.T., and Hemmati, M. (2000a) ‘Strong’ and ‘superstrong’ liquids, and an approach to the perfect glass state via phase transition. *Journal of Non-Crystalline Solids*, 274, 319–331.
- Angell, C.A., Ngai, K.L., McKenna, G.B., McMillan, P.F., and Martin, S.W. (2000b) Relaxation in glassforming liquids and amorphous solids. *Journal of Applied Physics*, 88, 3113–3157.
- Bagdasarov, N., Dorfman, A., and Dingwell, D.B. (2000) Effects of alkalis, phosphorus and water on surface tension of haplogranite melt. *American Mineralogist*, 85, 33–40.
- Blöchl, P.E. (1994) Projector augmented-wave method. *Physical Review B: Condensed Matter*, 50, 17953–17979.

- Blundy, J., and Dalton, J. (2000) Experimental comparison of trace element partitioning between clinopyroxene and melt in carbonate and silicate systems, and implications for mantle metasomatism. *Contributions to Mineralogy and Petrology*, 139, 356–371.
- Böhmer, R., Ngai, K.L., Angell, C.A., and Plazek, D.J. (1993) Nonexponential relaxations in strong and fragile glass formers. *The Journal of Chemical Physics*, 99, 4201–4209.
- Brey, G.P., and Green, D.H. (1976) Solubility of CO₂ in olivine melilitite at high pressures and role of CO₂ in the Earth's upper mantle. *Contributions to Mineralogy and Petrology*, 55, 217–230.
- Brooker, R.A., Sparks, R.S.J., Kavanagh, J., and Field, M. (2011) The volatile content of hypabyssal kimberlite magmas: Some constraints from experiments on natural rock compositions. *Bulletin of Volcanology*, 73, 959–981.
- Brooker, R.A. (1998) The effect of CO₂ saturation on immiscibility between silicate and carbonate liquids: An experimental study. *Journal of Petrology*, 39, 1905–1915.
- Brooker, R.A., and Kjarsgaard, B.A. (2011) Silicate-carbonate liquid immiscibility and phase relations in the system SiO₂-Na₂O-Al₂O₃-CaO-CO₂ at 0.1–2.5 GPa with applications to carbonatite genesis. *Journal of Petrology*, 52, 1281–1305.
- Brooker, R.A., Kohn, S.C., Holloway, J.R., and McMillan, P.F. (2001) Structural controls on the solubility of CO₂ in silicate melts. Part II: IR characteristics of carbonate groups in silicate glasses. *Chemical Geology*, 174, 241–254.
- Cassir, M., McPhail, S.J., and Moreno, A. (2012) Strategies and new developments in the field of molten carbonates and high-temperature fuel cells in the carbon cycle. *International Journal of Hydrogen Energy*, 37, 19345–19350.
- Dalton, J.A., and Wood, B.J. (1993) The compositions of primary carbonate melts and their evolution through wallrock reaction in the mantle. *Earth and Planetary Science Letters*, 119, 511–525.
- Dasgupta, R., and Hirschmann, M.M. (2010) The deep carbon cycle and melting in Earth's interior. *Earth and Planetary Science Letters*, 298, 1–13.
- Datta, R.K., Roy, D.M., Fails, S.P., and Tuttle, O.F. (1964) Glass formation in carbonate systems. *Journal of the American Ceramic Society*, 47, 153–153.
- Dawson, J.B. (1966) Oldoinyo Lengai—An active volcano with sodium carbonatite lava flows in carbonatites, p. 155–168. Wiley.
- Desmaele, E., Sator, N., Vuilleumier, R., and Guillot, B. (2019a) The MgCO₃-CaCO₃-Li₂CO₃-Na₂CO₃-K₂CO₃ melts: Thermodynamics and transport properties by atomistic simulations. *The Journal of Chemical Physics*, 150, 214503.
- (2019b) Atomistic simulations of molten carbonates: Thermodynamic and transport properties of the Li₂CO₃-Na₂CO₃-K₂CO₃ system. *The Journal of Chemical Physics*, 150, 094504.
- Di Genova, D., Romano, C., Hess, K.U., Vona, A., Poe, B.T., Giordano, D., Dingwell, D.B., and Behrens, H. (2013) The rheology of peralkaline rhyolites from Pantelleria Island. *Journal of Volcanology and Geothermal Research*, 249, 201–216.
- Di Genova, D., Cimarelli, C., Hess, K.U., and Dingwell, D.B. (2016) An advanced rotational rheometer system for extremely fluid liquids up to 1273 K and applications to alkali carbonate melts. *American Mineralogist*, 101, 953–959.
- Dingwell, D.B. (1996) Volcanic dilemma: Flow or blow? *Science*, 273, 1054–1055.
- Dingwell, D.B., Knoche, R., and Webb, S.L. (1993) A volume temperature relationship for liquid GeO₂ and some geophysically relevant derived parameters for network liquids. *Physics and Chemistry of Minerals*, 19, 445–453.
- Dingwell, D.B., Courtial, P., Giordano, D., and Nichols, A.R.L. (2004) Viscosity of peridotite liquid. *Earth and Planetary Science Letters*, 226, 127–138.
- Dobson, D.P., Jones, A.P., Rabe, R., Sekine, T., Kurita, K., Taniguchi, T., Kondo, T., Kato, T., Shimomura, O., and Urakawa, S. (1996) In-situ measurement of viscosity and density of carbonate melts at high pressure. *Earth and Planetary Science Letters*, 143, 207–215.
- Dorfman, A., Hess, K.-U., and Dingwell, D. (1996) Centrifuge-assisted falling-sphere viscometry. *European Journal of Mineralogy*, 8, 507–514.
- Du, X., Wu, M., Tse, J.S., and Pan, Y. (2018) Structures and transport properties of CaCO₃ melts under Earth's mantle conditions. *ACS Earth and Space Chemistry*, 2, 1–8.
- Easteal, A.J., Wilder, J.A., Mohr, R.K., and Moynihan, C.T. (1977) Heat capacity and structural relaxation of enthalpy in As₂Se₃ glass. *Journal of the American Ceramic Society*, 60, 134–138.
- Eitel, W., and Skalics, W. (1929) Double carbonates of alkalis and alkaline earths. *Zeitschrift für Anorganische und Allgemeine Chemie*, 183, 263–286.
- Ejima, T., Sato, Y., Yaegashi, S., and Kijima, T. (1984) Proceedings of the 17th Molten Salts Chemistry Symposium, 17th ed., 29 p. The Molten Salt Committee of The Electrochemical Society of Japan, Kobe 657, Japan.
- Förland, T., and Weyl, W.A. (1950) Formation of a sulfate glass. *Journal of the American Ceramic Society*, 33, 186–188.
- Fulcher, G.S. (1925) Analysis of recent measurements of the viscosity of glasses. *Journal of the American Ceramic Society*, 8, 339–355.
- Gaillard, F., Malki, M., Iacono-Marziano, G., Pichavant, M., and Scaillet, B. (2008) Carbonatite melts and electrical conductivity in the asthenosphere. *Science*, 322, 1363–1365.
- Genge, M.J., Jones, A.P., and Price, G.D. (1995) An infrared and Raman study of carbonate glasses: Implications for the structure of carbonatite magmas. *Geochimica et Cosmochimica Acta*, 59, 927–937.
- Gibbs, J.H., and Adam, G. (1965) On the temperature dependence of cooperative relaxation properties in glass-forming liquids. *The Journal of Chemical Physics*, 43, 139–146.
- Giordano, D., and Dingwell, D.B. (2003) Viscosity of hydrous Etna basalt: Implications for Plinian-style basaltic eruptions. *Bulletin of Volcanology*, 65, 8–14.
- Giordano, D., Russell, J.K., and Dingwell, D.B. (2008) Viscosity of magmatic liquids: A model. *Earth and Planetary Science Letters*, 271, 123–134.
- Giordano, D., Ardia, P., Romano, C., Dingwell, D.B., Di Muro, A., Schmidt, M.W., Mangiacapra, A., and Hess, K.U. (2009) The rheological evolution of alkaline Vesuvius magmas and comparison with alkaline series from the Phlegrean Fields, Etna, Stromboli and Teide. *Geochimica et Cosmochimica Acta*, 73, 6613–6630.
- Gittins, J., and Jago, B.C. (1991) Extrusive carbonatites: Their origins reappraised in the light of new experimental data. *Geological Magazine*, 128, 301–305.
- Gottsmann, J., Giordano, D., and Dingwell, D.B. (2002) Predicting shear viscosity during volcanic processes at the glass transition: A calorimetric calibration. *Earth and Planetary Science Letters*, 198, 417–427.
- Gudfinnsson, G.H., and Presnall, D.C. (2005) Continuous gradations among primary carbonatitic, kimberlitic, melilititic, basaltic, picritic, and komatiitic melts in equilibrium with garnet lherzolite at 3–8 GPa. *Journal of Petrology*, 46, 1645–1659.
- Hammouda, T., and Laporte, D. (2000) Ultrafast mantle impregnation by carbonatite melts. *Geology*, 28, 283–285.
- Hess, K.U., and Dingwell, D.B. (1996) Viscosities of hydrous leucogranitic melts: a non-Arrhenian model. *American Mineralogist*, 81, 1297–1300.
- Hess, K.U., Dingwell, D.B., and Webb, S.L. (1995) The influence of excess alkalis on the viscosity of a haplogranitic melt. *American Mineralogist*, 80, 297–304.
- Hetherington, G., Jack, K.H., and Kennedy, (1964) The viscosity of vitreous silica. *Physics and Chemistry of Glasses*, 5, 130–136.
- Hofmaier, G., and Urbain, G. (1968) *Science of Ceramics*. British Ceramic Society, Stoke-on-Trent.
- Hunter, R.H., and McKenzie, D. (1989) The equilibrium geometry of carbonate melts in rocks of mantle composition. *Earth and Planetary Science Letters*, 92, 347–356.
- Hurt, S.M., and Lange, R.A. (2019) The density of Li₂CO₃-Na₂CO₃-K₂CO₃-Rb₂CO₃-Cs₂CO₃-CaCO₃-SrCO₃-BaCO₃ liquids: New measurements, ideal mixing, and systematic trends with composition. *Geochimica et Cosmochimica Acta*, 248, 123–137.
- Ihinger, P. (1991) The interaction of water with granitic melt. Ph.D. dissertation, California Institute of Technology, Pasadena.
- Janz, G.J., and Lorenz, M.R. (1961) Molten carbonate electrolytes: Physical properties, structure, and mechanism of electrical conductance. *Journal of the Electrochemical Society*, 108, 1052.
- Janz, G.J., Yamamura, T., and Hansen, M.D. (1989) Corresponding-states data correlations and molten salts viscosities. *International Journal of Thermophysics*, 10, 159–171.
- Jones, A.P., and Wyllie, P.J. (1983) Low-temperature glass quenched from a synthetic, rare earth carbonatite: Implications for the origin of the Mountain Pass deposit. *Economic Geology*, 78, 1721–1723.
- Kargel, J.S., Kirk, R.L., Fegley, B. Jr. and Treiman, A.H. (1994) Carbonate-sulfate volcanism on Venus? *Icarus*, 112, 219–252.
- Keller, J. (1989) Extrusive carbonatites and their significance. *Carbonatites: Genesis and Evolution*, 70–88.
- Kim, S.W., Uematsu, K., Toda, K., and Sato, M. (2015) Viscosity analysis of alkali metal carbonate molten salts at high temperature. *Journal of the Ceramic Society of Japan*, 123, 355–358.
- Knoche, R., Webb, S.L., and Dingwell, D.B. (1992) Temperature dependent expansivities for silicate melts. A calorimetric and dilatometric study of the CaMgSi₂O₆-CaAl₂Si₂O₆ system. *Geochimica et Cosmochimica Acta*, 56, 689–699.
- Knoche, R., Dingwell, D.B., and Webb, S.L. (1995) Leucogranitic and pegmatitic melt densities: partial molar volumes for SiO₂, Al₂O₃, Na₂O, K₂O, Rb₂O, Cs₂O, Li₂O, BaO, SrO, CaO, MgO, TiO₂, B₂O₃, P₂O₅, F₂O₃, Ta₂O₅, Nb₂O₅, and WO₃. *Geochimica et Cosmochimica Acta*, 59, 4645–4652.
- Kohara, S., Akola, J., Morita, H., Suzuya, K., Weber, J.K.R., Wilding, M.C., and Benmore, C.J. (2011) Relationship between topological order and glass forming ability in densely packed enstatite and forsterite composition glasses. *Proceedings of the National Academy of Sciences*, 108, 14780–14785.
- Kono, Y., Kenney-Benson, C., Hummer, D., Ohfuji, H., Park, C., Shen, G., Wang, Y., Kavner, A., and Manning, C.E. (2014) Ultralow viscosity of carbonate melts at high pressures. *Nature Communications*, 5, 5091–5098.
- Kono, Y., Kenney-Benson, C., Shibasaki, Y., Park, C., Shen, G., and Wang, Y. (2015) High-pressure viscosity of liquid Fe and FeS revisited by falling sphere viscometry using ultrafast X-ray imaging. *Physics of the Earth and Planetary Interiors*, 241, 57–64.
- Kresse, G., and Furthmüller, J. (1996a) Efficiency of ab-initio total energy calculations for metals and semiconductors using a plane-wave basis set. *Computational Materials Science*, 6, 15–50.
- (1996b) Efficient iterative schemes for ab initio total-energy calculations using a plane-wave basis set. *Physical Review B: Condensed Matter and Materials Physics*, 54, 11169–11186.
- Lange, R.A., and Carmichael, I.S.E. (1987) Densities of Na₂O-K₂O-MgO-MgO-FeO-Fe₂O₃-Al₂O₃-TiO₂-SiO₂ liquids: New measurements and derived partial molar properties. *Geochimica et Cosmochimica Acta*, 51, 2931–2946.
- Liu, Q., and Lange, R.A. (2003) New density measurements on carbonate liquids and the partial molar volume of the CaCO₃ component. *Contributions to Mineralogy and Petrology*, 146, 370–381.
- Liu, Q., Tenner, T.J., and Lange, R.A. (2007) Do carbonate liquids become denser than

- silicate liquids at pressure? Constraints from the fusion curve of K_2CO_3 to 3.2 GPa. *Contributions to Mineralogy and Petrology*, 153, 55–66.
- MacFarlane, D.R. (1984) Attempted glass formation in pure KH_2SO_4 . *Journal of the American Ceramic Society*, 67, C-28–C-28.
- McKenzie, D. (1985) The extraction of magma from the crust and mantle. *Earth and Planetary Science Letters*, 74, 81–91.
- Minarik, W.G., and Watson, E.B. (1995) Interconnectivity of carbonate melt at low melt fraction. *Earth and Planetary Science Letters*, 133, 423–437.
- Morizet, Y., Paris, M., Sifré, D., Di Carlo, I., Ory, S., and Gaillard, F. (2017) Towards the reconciliation of viscosity change and CO_2 -induced polymerisation in silicate melts. *Chemical Geology*, 458, 38–47.
- Moynihan, C.T. (1993) Correlation between the width of the glass transition region and the temperature dependence of the viscosity of high- T_g glasses. *Journal of the American Ceramic Society*, 76, 1081–1087.
- (2019) Structural relaxation and the glass transition. *Structure, Dynamics, and Properties of Silicate Melts*, 32, 1–19. *Reviews in Mineralogy & Geochemistry*.
- Moynihan, C.T., Eastaek, A.J., Bolt, M.A., and Tucker, J. (1976) Dependence of the fictive temperature of glass on cooling rate. *Journal of the American Ceramic Society*, 59, 12–16.
- Namiki, A., and Manga, M. (2008) Transition between fragmentation and permeable outgassing of low viscosity magmas. *Journal of Volcanology and Geothermal Research*, 169, 48–60.
- Nichols, A.R.L., Potuzak, M., and Dingwell, D.B. (2009) Cooling rates of basaltic hyaloclastites and pillow lava glasses from the HSDP2 drill core. *Geochimica et Cosmochimica Acta*, 73, 1052–1066.
- Norton, G., and Pinkerton, H. (1997) Rheological properties of natrocarbonatite lavas from Oldoinyo Lengai, Tanzania. *European Journal of Mineralogy*, 9, 351–364.
- Nosé, S. (1984) A unified formulation of the constant temperature molecular dynamics methods. *The Journal of Chemical Physics*, 81, 511–519.
- O’Leary, M.C., Lange, R.A., and Ai, Y. (2015) The compressibility of CaCO_3 - Li_2CO_3 - Na_2CO_3 - K_2CO_3 liquids: Application to natrocarbonatite and CO_2 -bearing nephelinitic liquids from Oldoinyo Lengai. *Contributions to Mineralogy and Petrology*, 170, 3.
- Perdew, J.P., Burke, K., and Ernzerhof, M. (1996) Generalized gradient approximation made simple. *Physical Review Letters*, 77, 3865–3868.
- Ragone, S.E., Datta, R.K., Roy, D.M., and Tuttle, O.F. (1966) The system potassium carbonate-magnesium carbonate. *The Journal of Physical Chemistry*, 70, 3360–3361.
- Rault, J. (2000) Origin of the Vogel-Fulcher-Tammann law in glass-forming materials: The β bifurcation. *Journal of Non-Crystalline Solids*, 271, 177–217.
- Richert, P. (1984) Viscosity and configurational entropy of silicate melts. *Geochimica et Cosmochimica Acta*, 48, 471–483.
- Russell, J.K., Giordano, D., and Dingwell, D.B. (2003) High-temperature limits on viscosity of non-Arrhenian silicate melts. *American Mineralogist*, 88, 1390–1394.
- Sato, Y., Yaegashi, S., Kijima, T., Takeuchi, E., Tamai, K., Hasebe, M., Hoshi, M., and Yamamura, T. (1999) Viscosities of molten alkali carbonates. *Netsu Bussei*, 13, 156–161.
- Scherer, G.W. (2006) Use of the Adam-Gibbs equation in the analysis of structural relaxation. *Journal of the American Ceramic Society*, 67, 504–511.
- Sharma, S.K., and Simons, B. (1980) Raman study of K_2CO_3 - MgCO_3 glasses. In H.S. Yoder, Ed., *Carnegie Institute of Washington Yearbook*, 79, 322–326. The Carnegie Institution of Washington, Washington D.C.
- Sifré, D., Gardés, E., Massuyeau, M., Hashim, L., Hier-Majumder, S., and Gaillard, F. (2014) Electrical conductivity during incipient melting in the oceanic low-velocity zone. *Nature*, 509, 81–85.
- Sifré, D., Hashim, L., and Gaillard, F. (2015) Effects of temperature, pressure and chemical compositions on the electrical conductivity of carbonated melts and its relationship with viscosity. *Chemical Geology*, 418, 189–197.
- Simandl, G.J., and Paradis, S. (2018) Carbonatites: related ore deposits, resources, footprint, and exploration methods. *Applied Earth Science*, 127, 123–152.
- Smyth, F.H., and Adams, L.H. (1923) The system, calcium oxide-carbon dioxide. *Journal of the American Chemical Society*, 45, 1167–1184.
- Stagno, V., Stopponi, V., Kono, Y., Manning, C.E., and Irifune, T. (2018) Experimental determination of the viscosity of Na_2CO_3 melt between 1.7 and 4.6 GPa at 1200–1700 °C: Implications for the rheology of carbonatite magmas in the Earth’s upper mantle. *Chemical Geology*, 501, 19–25.
- Stevenson, R.J., Dingwell, D.B., Webb, S.L., and Bagdassarov, N.S. (1995) The equivalence of enthalpy and shear stress relaxation in rhyolitic obsidians and quantification of the liquid-glass transition in volcanic processes. *Journal of Volcanology and Geothermal Research*, 68, 297–306.
- Tangeman, J.A., Phillips, B.L., Navrotsky, A., Weber, J.K.R., Hixson, A.D., and Key, T.S. (2001) Vitreous forsterite (Mg_2SiO_4): Synthesis, structure, and thermochemistry. *Geophysical Research Letters*, 28, 2517–2520.
- Thomson, A.R., Walter, M.J., Kohn, S.C., and Brooker, R.A. (2016) Slab melting as a barrier to deep carbon subduction. *Nature*, 529, 76–79.
- Treiman, A.H., and Schedl, A. (1983) Properties of carbonatite magma and processes in carbonatite magma chambers. *The Journal of Geology*, 91, 437–447.
- Tweer, H., Laberge, N., and Macedo, P.B. (1971) Inadequacies of viscosity theories for a vitreous KNO_3 - $\text{Ca(NO}_3)_2$ melt. *Journal of the American Ceramic Society*, 54, 121–123.
- Van Uiter, L.G., and Grodkiewicz, W.H. (1971) Nitrate glasses. *Materials Research Bulletin*, 6, 283–291.
- Vogel, H. (1921) The law of the relation between the viscosity of liquids and the temperature. *Physikalische Zeitschrift*, 22, 645–646.
- Vuilleumier, R., Seitsonen, A., Sator, N., and Guillot, B. (2014) Structure, equation of state and transport properties of molten calcium carbonate (CaCO_3) by atomistic simulations. *Geochimica et Cosmochimica Acta*, 141, 547–566.
- Wallace, M.E., and Green, D.H. (1988) An experimental determination of primary carbonatite magma composition. *Nature*, 335, 343–346.
- Weidner, J.R. (1972) Equilibria in the system Fe-C-O: Part I, Siderite-magnetite-carbon-vapor equilibrium from 500 to 10,000 bars. *American Journal of Science*, 272, 735–751.
- Weiler, R., Blaser, S., and Macedo, P.B. (1969) Viscosity of a vitreous potassium nitrate-calcium nitrate mixture. *The Journal of Physical Chemistry*, 73, 4147–4151.
- Whittington, A., Richet, P., Linard, Y., and Holtz, F. (2001) The viscosity of hydrous phonolites and trachytes. *Chemical Geology*, 174, 209–223.
- Wilding, M.C., Dingwell, D., Batiza, R., and Wilson, L. (2000) Cooling rates of hyaloclastites: Applications of relaxation geospeedometry to undersea volcanic deposits. *Bulletin of Volcanology*, 61, 527–536.
- Wilding, M.C., Wilson, M., Alderman, O.L.G., Benmore, C., Weber, J.K.R., Parise, J.B., Tamaloni, A., and Skinner, L. (2016) Low-dimensional network formation in molten sodium carbonate. *Scientific Reports*, 6, 24415.
- Wilding, M.C., Wilson, M., Ribeiro, M.C.C., Benmore, C.J., Weber, J.K.R., Alderman, O.L.G., Tamaloni, A., and Parise, J.B. (2017) The structure of liquid alkali nitrates and nitrites. *Physical Chemistry Chemical Physics*, 19, 21625–21638.
- Wilding, M.C., Bingham, P.A., Wilson, M., Kono, Y., Drewitt, J.W.E., Brooker, R.A., and Parise, J.B. (2019a) CO_{3+} network formation in ultra-high pressure carbonate liquids. *Scientific Reports*, 9, 15416.
- Wilding, M.C., Phillips, B.L., Wilson, M., Sharma, G., Navrotsky, A., Bingham, P.A., Brooker, R., and Parise, J.B. (2019b) The structure and thermochemistry of K_2CO_3 - MgCO_3 glass. *Journal of Materials Research*, 34, 3377–3388.
- Wilson, M., Ribeiro, M.C.C., Wilding, M.C., Benmore, C., Weber, J.K.R., Alderman, O., Tamaloni, A., and Parise, J.B. (2018) Structure and liquid fragility in sodium carbonate. *The Journal of Physical Chemistry A*, 122, 1071–1076.
- Wu, Y.T., Ren, N., Wang, T., and Ma, C.F. (2011) Experimental study on optimized composition of mixed carbonate salt for sensible heat storage in solar thermal power plant. *Solar Energy*, 85, 1957–1966.
- Wyllie, P.J., and Huang, W.L. (1976) Carbonation and melting reactions in the system $\text{CaO-MgO-SiO}_2\text{-CO}_2$ at mantle pressures with geophysical and petrological applications. *Contributions to Mineralogy and Petrology*, 54, 79–107.
- Yue, Y.Z. (2008) Characteristic temperatures of enthalpy relaxation in glass. *Journal of Non-Crystalline Solids*, 354, 1112–1118.
- Yue, Y., Von der Ohe, R., and Jensen, S.L. (2004) Fictive temperature, cooling rate, and viscosity of glasses. *The Journal of Chemical Physics*, 120, 8053–8059.
- Zimanowski, B., Lorenz, V., and Frohlich, G. (1986) Experiments on phreatomagmatic explosions with silicate and carbonatitic melts. *Journal of Volcanology and Geothermal Research*, 30, 149–153.
- Zimanowski, B., Büttner, R., and Nestler, J. (1997) Brittle reaction of a high-temperature ion melt. *Europhysics Letters*, 38, 285–289.

MANUSCRIPT RECEIVED AUGUST 12, 2020

MANUSCRIPT ACCEPTED AUGUST 17, 2021

MANUSCRIPT HANDLED BY YANN MORIZET

Endnote:

¹Deposit item AM-22-67752, Online Materials. Deposit items are free to all readers and found on the MSA website, via the specific issue’s Table of Contents (go to http://www.minsocam.org/MSA/AmMin/TOC/2022/Jun2022_data/Jun2022_data.html).